



# 3D-Printed Eosin Y-Based Heterogeneous Photocatalyst for Organic Reactions

Cloé Delacourt, Abraham Chemtob, Jean-Philippe Goddard, Arnaud Spangenberg, Morgan Cormier

## ► To cite this version:

Cloé Delacourt, Abraham Chemtob, Jean-Philippe Goddard, Arnaud Spangenberg, Morgan Cormier. 3D-Printed Eosin Y-Based Heterogeneous Photocatalyst for Organic Reactions. Chemistry - A European Journal, inPress, 10.1002/chem.202304363 . hal-04495132

**HAL Id: hal-04495132**

**<https://hal.science/hal-04495132>**

Submitted on 8 Mar 2024

**HAL** is a multi-disciplinary open access archive for the deposit and dissemination of scientific research documents, whether they are published or not. The documents may come from teaching and research institutions in France or abroad, or from public or private research centers.

L'archive ouverte pluridisciplinaire **HAL**, est destinée au dépôt et à la diffusion de documents scientifiques de niveau recherche, publiés ou non, émanant des établissements d'enseignement et de recherche français ou étrangers, des laboratoires publics ou privés.

# Chemistry A European Journal

 **Chemistry  
Europe**  
European Chemical  
Societies Publishing

## Accepted Article

**Title:** 3D-Printed Eosin Y-Based Heterogeneous Photocatalyst for Organic Reactions

**Authors:** Cloé Delacourt, Abraham Chemtob, Jean-Philippe Goddard, Arnaud Spangenberg, and Morgan Cormier

This manuscript has been accepted after peer review and appears as an Accepted Article online prior to editing, proofing, and formal publication of the final Version of Record (VoR). The VoR will be published online in Early View as soon as possible and may be different to this Accepted Article as a result of editing. Readers should obtain the VoR from the journal website shown below when it is published to ensure accuracy of information. The authors are responsible for the content of this Accepted Article.

**To be cited as:** *Chem. Eur. J.* **2024**, e202304363

**Link to VoR:** <https://doi.org/10.1002/chem.202304363>

WILEY-VCH

## COMMUNICATION

## 3D-Printed Eosin Y-Based Heterogeneous Photocatalyst for Organic Reactions

Cloé Delacourt,<sup>[a],[b]</sup> Abraham Chemtob,<sup>[b]</sup> Jean-Philippe Goddard,<sup>[a]</sup> Arnaud Spangenberg,<sup>\*,[b]</sup> Morgan Cormier<sup>\*,[a]</sup>

[a] Laboratoire d'Innovation Moléculaire et Applications (LIMA), UMR 7042  
Université de Haute-Alsace, Université de Strasbourg, CNRS  
3 rue Alfred Werner, 68093 Mulhouse  
E-mail: [morgan.cormier@uha.fr](mailto:morgan.cormier@uha.fr)

[b] Institut de Science des Matériaux de Mulhouse (IS2M) UMR 7361  
Université de Haute-Alsace, Université de Strasbourg, CNRS  
15 rue Jean Starcky, 68057 Mulhouse  
E-mail: [arnaud.spangenberg@uha.fr](mailto:arnaud.spangenberg@uha.fr)

Supporting information for this article is given via a link at the end of the document.

**Abstract:** Heterogenization of Eosin Y by 3D-printing and its application in photocatalysis are reported. The approach allows a fine tuning of the photocatalyst morphology and its rapid preparation. Photocatalytic activity was evaluated through model organic reactions involving oxidation, reduction, and photosensitization pathways. The efficiency, recyclability and stability of 3D printed EY is remarkable paving the way to new generation of heterogeneous photocatalysts with a perfect control of their shape and adaptable to any photoreactors.

Visible-light photocatalysis has recently emerged as a cutting-edge method to perform organic reactions.<sup>[1],[2],[3],[4],[5],[6]</sup> This approach requires a photocatalyst (PCat) able to promote a Single Electron Transfer (SET)<sup>[7]</sup> or an Energy Transfer (EnT)<sup>[8]</sup> at its excited state. The design and development of photocatalyst is now well established and a large panel of structures is currently accessible including transition metal complexes<sup>[9]</sup> or organic dyes.<sup>[10]</sup> The photocatalyst development allows a marked variation in redox properties and wavelengths (from UV to near Infrared<sup>[11–13]</sup>). However, most of the photocatalysts are prepared and used in homogeneous phase which limits the potential applications since the photocatalyst is difficult to recover after the reaction. One possible solution is to heterogenize it on an insoluble support.<sup>[14–16]</sup> To do so, various supports have been studied including silica materials,<sup>[17,18]</sup> MOFs,<sup>[19]</sup> metal particles,<sup>[20]</sup> and polymers. Polymeric supports present interesting features such as transparency, simple preparation, and versatile functionalization. The photocatalyst can be grafted at the surface of the polymer or embedded.<sup>[21,22]</sup> Conjugated polymers are also be considered as a valuable solution to obtain polymer-based heterogeneous photocatalysts.<sup>[23,24]</sup> Whatever the support, the heterogeneous photocatalyst is usually obtained in the form of powder and the recycling process is performed by filtration or centrifugation. Thus, the photocatalysis gains in sustainability by catalyst recovering at the end of the reaction. To go further, it would be interesting to control the shaping of the heterogeneous photocatalyst, enhancing its recyclability and enabling better adaptation to a photoreactor. The morphology control of the

photocatalyst at the macroscopic scale is a crucial parameter which is not often considered.

In parallel the 3D-printing concept has also emerged over the last few years.<sup>[25]</sup> This technology is still under development, but it allows the photopolymerization of huge variety of objects with a high degree of precision.<sup>[26–28]</sup> Recently, this field of research has been applied to produce catalysts with different shapes. 3D-printed objects were prepared for organometallic/organocatalysts at their ground state.<sup>[29–34]</sup> In contrast, very few examples of photocatalysts on 3D-printed objects have been reported and they are mainly based on inorganic particle<sup>[35,36]</sup> or obtained by post-grafting<sup>[37]</sup>. Thus, a general approach to directly 3D-print a photocatalyst is currently missing. We thought that this technology could be applied to photocatalysts in order to obtain well defined heterogeneous systems able to perform organic reactions. The challenge is to use the photopolymerization technology to print a photocatalyst which is itself photoactive. This point must be considered since the polymerization could be affected and the photodegradation of the photocatalyst could occur. As shown in Figure 1, two approaches were investigated herein, the physical trapping of the photocatalyst inside the polymer matrix during the photopolymerization or the covalent linkage of the PCat onto the support surface. This last strategy requires a modification of the PCat to incorporate a polymerizable function.

## This work

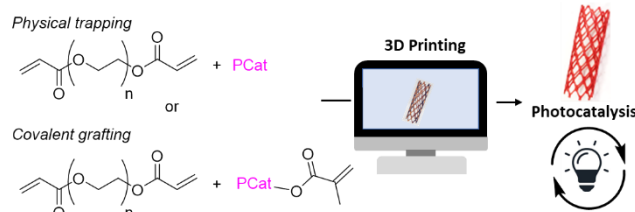


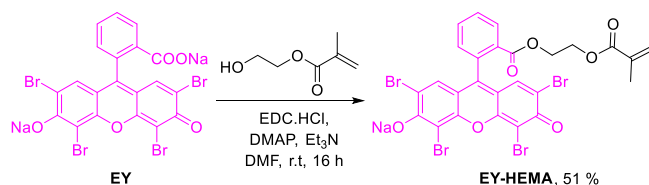
**Figure 1.** The concept of 3D-printed photocatalyst.

In this work, we have selected Eosin Y (EY) as a PCat. EY is a versatile, accessible, stable, and easily tunable catalyst.<sup>[38,39]</sup> It was heterogenized on polymer supports to obtain various catalytic systems mainly as a powder.<sup>[40–44]</sup> To go further and

## COMMUNICATION

obtain well defined heterogeneous EY-based PCat, we investigated its preparation using 3D-printing technology.

First, we decided to modify **EY** in order to evaluate both strategies (physical trapping and covalent grafting). To do so, we chose to derivatize the **EY** with a methacrylate polymerizable group. To prepare the reactive **EY** derivative, 2-hydroxyethyl methacrylate (HEMA) was reacted with **EY** using EDC/DMAP coupling conditions in 51 % isolated yield (Scheme 1).<sup>[43]</sup> After performing UV-visible and fluorescence spectroscopies on **EY-HEMA** only few differences were observed between **EY** and **EY-HEMA** (see ESI Fig.S1).



**Scheme 1.** Synthesis of **EY-HEMA**

Then, we explored the heterogenization of **EY** and **EY-HEMA** using a DLP 3D printer. Polyethylene glycol diacrylate (PEGDA) was used as a precursor to prepare the crosslinked polymer support. PEGDA has the advantage of easy polymerization, transparency, low viscosity facilitating 3D structuring, and a high swelling index, which can be interesting for catalyst accessibility. Phenylbis(2,4,6-trimethylbenzoyl)phosphine oxide (BAPO) was used as a radical photoinitiator for polymerization. To ensure good resolution during the 3D printing process (25 – 300  $\mu\text{m}$  layer thickness), the Jacobs working curve<sup>[45–47]</sup> based on experimental measurements must be established before conducting a DLP print. This curve highlights the correlation between absorbed light energy  $E$  for a layer and the cured thickness  $C_d$  of the photosensitive material during exposure to light. Using the Beer-Lambert law, Jacobs laid out the principles of stereolithography and provided an equation for this working curve (Equation 1), with  $D_p$  the depth of light penetration and  $E_c$  the critical exposure energy defined as the minimum energy dose to form a film.

$$C_d = D_p \times \ln\left(\frac{E}{E_c}\right) \quad (\text{Eq. 1})$$

To further regulate the Jacobs' working curve, photoabsorbers, i.e. dyes<sup>[48,49]</sup> or quenchers,<sup>[50,51]</sup> are used. Since **EY** acts as a light absorber, we initially established Jacobs' curves for various formulations in **EY** (0.8 – 4 wt%). The low solubility (see ESI Fig.S2) of **EY** in PEDGA did not allow for good incorporation into the resin. To achieve higher **EY** loadings, ethanol (EtOH, 10 wt%) was added to the resin to improve miscibility between the photocatalyst and the polymer. However, to maintain both good resolution and a short printing time, the optimal percentage of **EY** is 3 wt% (see ESI Fig.S3). As shown in Figure 2a, **EY-HEMA** plays a similar role as an absorber, resulting in z-confinement of the polymerization reaction. However, a closer analysis reveals a difference in reactivity between **EY** and **EY-HEMA**-based formulations resulting in a lower critical energy for **EY-HEMA** (34 vs. 36  $\text{mW}\cdot\text{cm}^{-2}\cdot\text{s}$ , see ESI Fig. S4). This can be explained by the fact that **EY-HEMA** has a slightly lower molar extinction coefficient than **EY** (1370 vs 2540  $\text{L}\cdot\text{mol}^{-1}\cdot\text{cm}^{-1}$ ) at the printing wavelength (i.e. 385 nm), and that the molar amount of **EY-HEMA** introduced into the reaction is slightly lower (1.53 vs

1.73 mmol). However, only a slight difference was observed in the photopolymerization kinetics illustrated by the fact that degrees of conversion and maximum polymerization rates were similar (Figure 2b and ESI Tab. S1). Therefore, the mass percentage of **EY-HEMA** in the formulation was set at 3 wt% for the entire study.

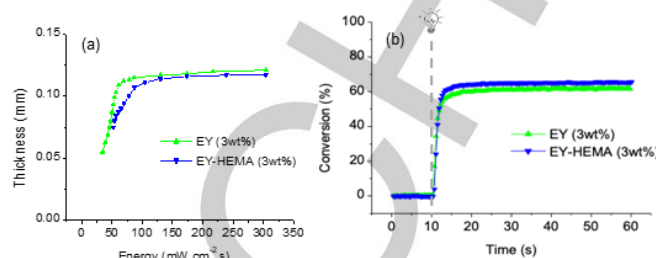


**Figure 2 .** (a) Jacobs working curves for an acrylate formulation containing 3 wt% of **EY** (i.e. 1.73 mmol, Green) and 3 wt% of **EY-HEMA** (i.e. 1.53 mmol, Blue), (b) Photopolymerization experiments by RT-FTIR using 3 wt% **EY** or 3 wt% **EY-HEMA** under LED 365 nm and 75  $\text{mW}\cdot\text{cm}^{-2}$  of incident irradiance.

Then our attention has been directed towards the design of devices with precise shapes that can be manufactured through the 3D printing process. Considering that increased catalytic performances can result from an increase in contact surfaces, and the ease of reusing the supported photocatalyst, we targeted on a specific shape: a stent fitting around a magnetic stirring bar (20 x 6 mm) as illustrated in Figure 1.

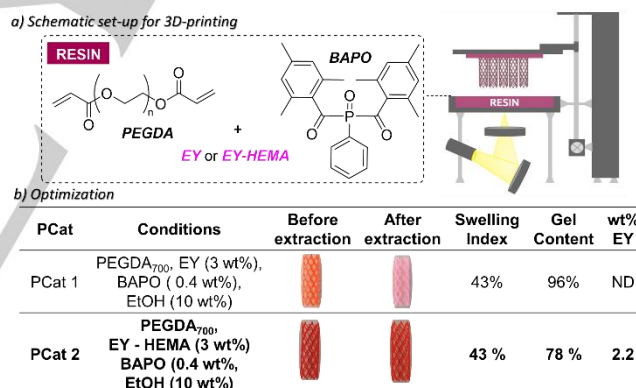


**Figure 3 .** Preparation of 3D-printed **EY**-based photocatalyst

Next, a preparation of 40 g of resin was carried out for each formulation, including 0.4 wt% of BAPO, 10 wt% of EtOH, and 3 wt% of **EY** or **EY-HEMA**. Based on the experimental measurements obtained from Jacobs' working curves, the 3D printing process was implemented with a layer thickness of 50  $\mu\text{m}$  for **EY** and 75  $\mu\text{m}$  for **EY-HEMA**. The stents were printed vertically, eliminating the need of supports during printing. In order to assess CAD fidelity, SEM images of **EY-HEMA** stents were performed (see ESI Fig.S7). While the layer thickness was set at 75  $\mu\text{m}$ , the printed stent features layers with a thickness of 70  $\mu\text{m}$ , less than 10% different from the CAD model.

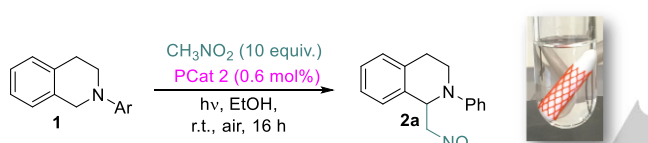
Moreover, this small difference can be partly attributed to shrinkage of the structure, favored by the vacuum conditions in the SEM chamber. Multiple copies of the devices were printed simultaneously on the same build plate to ensure efficient production. The printed objects were then washed before use, removing any residue of unpolymerized material (conversions








## COMMUNICATION

63% and 66% for **EY** and **EY-HEMA**, respectively, Figure 2b) as well as untrapped eosin that could lead to homogeneous phase catalysis. For this purpose, the stents were washed by Soxhlet extraction in EtOH for 24 hours. After this process, the devices were vacuum dried to a constant weight. This enabled gel content to be determined and eosin content to be estimated by UV spectroscopic analysis of the extraction filtrate. Unfortunately, due to the weak bond between the photocatalyst and the polymer during physical trapping, we observed significant leaching of **EY** for **PCat 1** (Figure 3). On the contrary, the formulation containing **EY-HEMA** allows to significantly decrease its leaching after polymerization since **EY** is now covalently bounded to the support. These conditions are efficient to get a stent grafted with **EY** and the loading was estimated to 2.2 wt% (Figure 3, **PCat 2**). We tested the stability of **PCat 2** in various solvents and we found that these objects are perfectly stable in ethanol and acetonitrile without any traces of leaching (see ESI Fig.S8). This stability is reinforced by this high gel content value measured on **PCat 2** (78 %). For this photocatalyst, a swelling index of 43 % was determined suggesting that **EY** should be accessible for small organic molecules.

**Table 1.** Optimization of the reaction conditions



Entry	Conditions	Conv. (%) <sup>[a]</sup>	Photo-bleaching
1	C = 0.15 mmol/L, green LED, <sup>[b]</sup> 24 h	54	Yes 
2	C = 0.3 mmol/L, green LED, <sup>[b]</sup> 16 h	100	No 
3	C = 0.15 mmol/L, blue LED, <sup>[c]</sup> 24 h	71	No 
4	C = 0.3 mmol/L, blue LED, <sup>[c]</sup> 16 h	100	No 
5	C = 0.3 mmol/L, blue LED, <sup>[d]</sup> 24 h	42	No 
6	No PCat, blue LED, <sup>[c]</sup> 16 h	16	-
7	C = 0.3 mmol/L, dark, 16 h	3	-
8	0.2 mol% BAPO, blue LED, <sup>[c]</sup> 16 h	34	-

<sup>[a]</sup> Reactions were run on 0.1 mmol scale and conversion determined by <sup>1</sup>H-NMR on the crude. <sup>[b]</sup> 565 nm, 11.7 μW/mm<sup>2</sup>. <sup>[c]</sup> 455 nm, 32 μW/mm<sup>2</sup>. <sup>[d]</sup> 455 nm, 10 μW/mm<sup>2</sup>

Next, we explored the photocatalytic activity of **PCat 2** using the oxidation of *N*-aryltetrahydroisoquinoline **1** to perform the aza-Henry reaction with nitromethane. Since the  $\lambda_{\max}$  absorption of **EY-HEMA** in EtOH was measured at 540 nm, we explored this reaction using a green LED (565 nm). Under these conditions 54 % of **2a** was obtained after 16 h of irradiation in EtOH under air. However, this first result was tarnished by a partial degradation of the photocatalyst, a strong photobleaching was observed (Table 1, entry 1). Then the reaction was concentrated to 0.3 M to improve the kinetic and decrease the irradiation time. Under these conditions, full conversion was reached, and no apparent photobleaching was noted (Table 1, entry 2). In parallel, we investigated the reaction upon irradiation with blue LED (455

nm). Indeed, the photobleaching of **EY** can occur by various mechanisms and the impact of wavelength could be important.<sup>[52]</sup> To learn more about the effect of irradiation conditions, blue light irradiation was implemented at two different irradiances, 32 μW/mm<sup>2</sup> and 10 μW/mm<sup>2</sup> (Table 1, entries 3,4,5). The best conditions (455 nm, 32 μW/mm<sup>2</sup>, 16 h) gave **2** very efficiently, without any apparent photobleaching of the **EY**. Then a series of control reactions were run to secure the role of the photocatalyst in the reaction. In the dark or without photocatalyst, very low conversions were observed (3 % and 16 %). Finally, we verified if the BAPO can play the role of photocatalyst in this reaction. In principle, BAPO should be totally consumed after the photopolymerization, but few traces could remain. When we exposed **1**, to a large amount of BAPO, in the optimal conditions, we observed 34 % of conversion. This value is far to the full conversion observed in presence of **PCat 2** and cannot be higher since the concentration of BAPO in the heterogeneous photocatalyst should be very low.

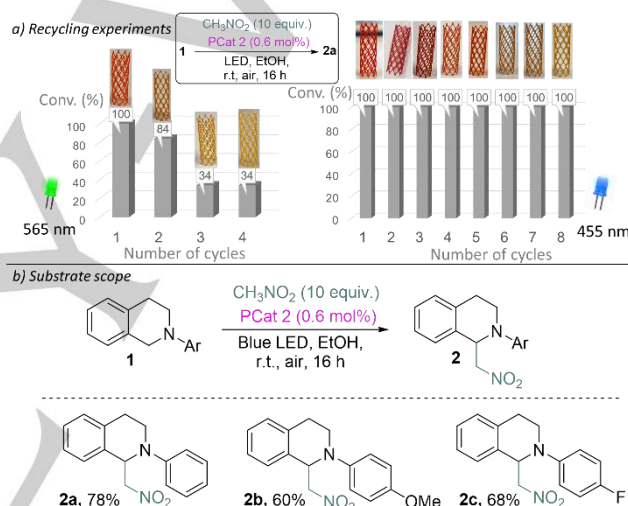


**Figure 4.** Aza-Henry reactions performed under green or blue LED excitation in presence of a 3D printed **EY** heterogeneous catalyst. a) Investigation of the recyclability of the printed photocatalyst. b) Substrate scope

To test the robustness of **PCat 2** we explored recycling experiments. The stent surrounding the magnetic stirring bar is easily recovered, rinsed with EtOH and dried under vacuum at the end of the reaction. Interesting, the results are totally different depending on the irradiation wavelength (565 nm or 455 nm). With the green LED (11.7 μW/mm<sup>2</sup>), only two cycles could be performed, after which **PCat 2** became yellow and not photoactive anymore (Figure 4a). However, using blue light LED (32 μW/mm<sup>2</sup>) we were able to perform more than 8 cycles without erosion of the conversion. Progressively the stent started to become yellow but the photobleaching appeared to be slow and enough catalytically active **EY** was still present to promote the reaction even after 8 cycles (Figure 4a). For all the reactions, very few by-products were observed but we decided to run a further step of purification to reach the highest purity. First, we verified if some products could be trapped inside the polymer but even after several rinses with EtOH only few traces of **2a** were detected (see ESI Fig.S10). Finally, neutral phenyl, electron rich methoxy and electron poor fluorine have been tested (Figure 4b) and we obtained similar results after purification: 78 % (**2a**), 60 % (**2b**), 68 % (**2c**). Parts of

## COMMUNICATION

the yields are impacted by the purification; this is due to low stability of **2** on silica.

**Table 2.** Reductive radical cyclization of bis-enone (**3**)

Entry	Conditions <sup>[a]</sup>	Yield <b>4a</b> (%) <sup>[b]</sup>	Yield <b>4b</b> (%) <sup>[b]</sup>
1	EY (homogeneous)	53	25
2	<b>PCat 2</b> , cycle 1	31	21
3	<b>PCat 2</b> , cycle 2	10	<5
4	No <b>PCat</b>	15	0
5	In the Dark	0	0

<sup>[a]</sup> Reactions were run on 0.1 mmol scale. Blue LED : 455 nm, 32  $\mu$ W/mm<sup>2</sup>.<sup>[b]</sup> NMR-yields are determined by <sup>1</sup>H-NMR on the crude reaction mixture using the diphenylethylene as internal standard.

Encouraged by these results of oxidation reactions, we decided to explore the reductive pathway. The reduction of the bis-enone (**3**) was selected as a model reaction. To perform this reaction, additives need to be added in the solution. Lithium bromide was used to activate the carbonyl scaffold while diisopropylethylamine (DIPEA) is necessary to promote catalytic cycle. This reaction was performed in absence of air in acetonitrile. Interestingly, after the first cycle we obtained a positive result, the radical cyclization was observed in 52 % global yield with a poor diastereoselectivity (**4a:4b**= 1.5) (Table 2, entry 2). To compare, the reaction in homogeneous phase gave a higher yield (78 %) (Table 1, entry 1), and a slightly different diastereomeric ratio (**4a:4b**= 2.1). However, these conditions seem to be harsher for the photocatalyst, since only one cycle could be performed with **PCat 2**, the yield dropped to 15 % after the second cycle. This could be explained by the formation of different C-radical intermediates under anaerobic conditions which can accelerate the photodegradation. It should be noted that stability tests have been performed on **PCat 2** in presence of DIPEA or LiBr, the photocatalyst appears to be stable (see ESI Fig.S8). In addition, it is important to notify that the support is not involved in the photodegradation of **EY**, control reaction have been performed in homogeneous phase (see ESI p.S11).

To demonstrate the versatility of **PCat 2**, we explored the ability of this photocatalyst to transfer energy (EnT) for the generation of singlet oxygen. To do so, we selected the oxidation of dimethylantracene (**5**) and the formation of the endo peroxide (**6**). Interestingly the oxidation of **3** occurred very efficiently giving **4** quantitatively even after 8 cycles (Figure 5). We confirmed the effect of **PCat 2** in the reaction through control reactions (see ESI p.S12). In this case the photocatalyst remained intact, demonstrating the high stability of **PCat 2** under strong oxidative conditions. We also verified if a potential degradation could affect the kinetic of the reaction, but after 35 min of reaction, the same conversions are observed from the cycle 1 to 5 (see ESI Fig.S11). This last result opens the door to many other applications in organic synthesis where <sup>1</sup>O<sub>2</sub> could be involved<sup>[53]</sup> but it could be

also considered for other applications involving this intermediate.<sup>[54]</sup>

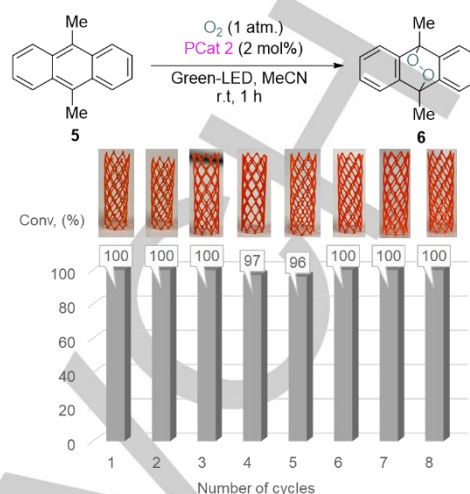


**Figure 5.** Photo-oxidation of dimethylantracene

In conclusion, after a simple modification of **EY** to incorporate a methacrylate function, the 3D-printed stent doped with this organic dye was obtained successfully. The stent was printed to fit with a magnetic stirring bar giving an easy recyclable photocatalyst. The photocatalytic activity as well as the stability of this photocatalyst was demonstrated through three types of reaction: oxidative aza-Henry reaction, reductive radical cyclization, and the generation of <sup>1</sup>O<sub>2</sub>. For these reactions, the printed **EY** were efficient even after several recycling steps. These results pave the way to further photocatalyst heterogenizations and a wide variety of objects could be considered with this technology to fit with diverse photoreactors.

## Acknowledgements

This work of the Interdisciplinary Institute HiFunMat, as part of the ITI 2021-2028 program of the University of Strasbourg, CNRS and Inserm, was supported by IdEx Unistra (ANR-10-IDEX-0002) and SFRI (STRAT'US project, ANR-20-SFRI-0012) under the framework of the French Investments for the Future Program. This work was supported by a French government grant managed by ANR under the France 2030 program (Project Mat-Light 4.0 - ANR-21-EXES-0012) The authors acknowledge the University de Haute-Alsace (UHA), the CNRS for providing facilities. The authors thank Dr. Didier Le Nouen responsible of the analytical platforms of LIMA (UMR7042 CNRS-Unistra-UHA) who contributed, by his valuable technical and scientific support, to the achievement of this research project.

**Keywords:** Photocatalysis • 3D-printing • Eosin Y • Heterogeneous catalysis.

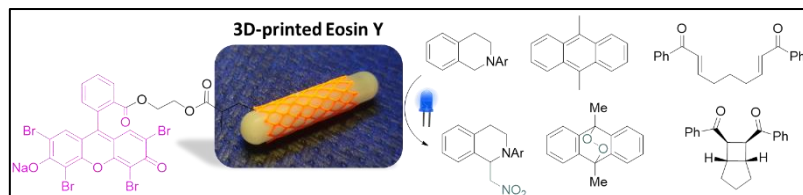
- [1] L. Candish, K. D. Collins, G. C. Cook, J. J. Douglas, A. Gómez-Suárez, A. Jolit, S. Keess, *Chem. Rev.* **2022**, 122, 2907–2980.
- [2] J. D. Bell, J. A. Murphy, *Chem. Soc. Rev.* **2021**, 50, 9540–9685.
- [3] R. C. McAtee, E. J. McClain, C. R. J. Stephenson, *Trends in Chemistry* **2019**, 1, 111–125.

## COMMUNICATION

- [4] M. H. Shaw, J. Twilton, D. W. C. MacMillan, *J. Org. Chem.* **2016**, *81*, 6898–6926.
- [5] R. A. Angnes, Z. Li, C. R. D. Correia, G. B. Hammond, *Org. Biomol. Chem.* **2015**, *13*, 9152–9167.
- [6] D. A. Nicewicz, T. M. Nguyen, *ACS Catal.* **2014**, *4*, 355–360.
- [7] N. E. S. Tay, D. Lehnher, T. Rovis, *Chem. Rev.* **2022**, *122*, 2487–2649.
- [8] F. Strieth-Kalthoff, M. J. James, M. Teders, L. Pitzer, F. Glorius, *Chem. Soc. Rev.* **2018**, *47*, 7190–7202.
- [9] C. K. Prier, D. A. Rankic, D. W. C. MacMillan, *Chem. Rev.* **2013**, *113*, 5322–5363.
- [10] N. A. Romero, D. A. Nicewicz, *Chem. Rev.* **2016**, *116*, 10075–10166.
- [11] N. Sellet, M. Cormier, J.-P. Goddard, *Org. Chem. Front.* **2021**, *10*, 1039.D1QO01476E.
- [12] A. R. Obah Kosso, N. Sellet, A. Baralle, M. Cormier, J.-P. Goddard, *Chem. Sci.* **2021**, *12*, 6964–6968.
- [13] N. Sellet, M. Sebbat, M. Elhabiri, M. Cormier, J.-P. Goddard, *Chem. Commun.* **2022**, *58*, 13759–13762.
- [14] X. Lang, X. Chen, J. Zhao, *Chem. Soc. Rev.* **2014**, *43*, 473–486.
- [15] S. Gisbertz, B. Pieber, *ChemPhotoChem* **2020**, *4*, 456–475.
- [16] M. Cherevatskaya, B. König, *Russ. Chem. Rev.* **2014**, *83*, 183–195.
- [17] S. M. Soria-Castro, B. Lebeau, M. Cormier, S. Neunlist, T. J. Daou, J.-P. Goddard, *Eur. J. Org. Chem.* **2020**, *2020*, 1572–1578.
- [18] N. Mahmoud, J. Awassa, J. Toufaily, B. Lebeau, T. J. Daou, M. Cormier, J.-P. Goddard, *Molecules* **2023**, *28*, 549.
- [19] S.-N. Zhao, G. Wang, D. Poelman, P. Van Der Voort, *Molecules* **2018**, *23*, 2947.
- [20] H. Cheng, W. Xu, *Org. Biomol. Chem.* **2019**, *17*, 9977–9989.
- [21] C. T. J. Ferguson, K. A. I. Zhang, *ACS Catal.* **2021**, *11*, 9547–9560.
- [22] C. Esen, B. Kumru, *Ind. Eng. Chem. Res.* **2022**, *61*, 10616–10630.
- [23] H. Zhang, W. Wei, K. A. I. Zhang, *Chem. Commun.* **2023**, *59*, 9167–9181.
- [24] J. Xiao, X. Liu, L. Pan, C. Shi, X. Zhang, J.-J. Zou, *ACS Catal.* **2020**, *10*, 12256–12283.
- [25] A. Bagheri, J. Jin, *ACS Appl. Polym. Mater.* **2019**, *1*, 593–611.
- [26] C. Barner-Kowollik, M. Bastmeyer, E. Blasco, G. Delaittre, P. Müller, B. Richter, M. Wegener, *Angew. Chem. Int. Ed.* **2017**, *56*, 15828–15845.
- [27] M. Belqat, X. Wu, J. Morris, K. Mougín, T. Petithory, L. Pieuchot, Y. Guillauneuf, D. Gimes, J. Clément, A. Spangenberg, *Adv. Funct. Materials* **2023**, 2211971.
- [28] X. Wu, B. Gross, B. Leuschel, K. Mougín, S. Dominici, S. Gree, M. Belqat, V. Tkachenko, B. Cabannes-Boué, A. Chemtob, J. Poly, A. Spangenberg, *Adv. Funct. Materials* **2022**, *32*, 2109446.
- [29] L. Chen, S. Zhou, M. Li, F. Mo, S. Yu, J. Wei, *Catalysts* **2022**, *12*, 1081.
- [30] M. R. Penny, S. T. Hilton, *React. Chem. Eng.* **2020**, *5*, 853–858.
- [31] A. S. Díaz-Marta, C. R. Tubío, C. Carbajales, C. Fernández, L. Escalante, E. Sotelo, F. Guitián, V. L. Barrio, A. Gil, A. Coelho, *ACS Catal.* **2018**, *8*, 392–404.
- [32] J. S. Manzano, Z. B. Weinstein, A. D. Sadow, I. I. Slowing, *ACS Catal.* **2017**, *7*, 7567–7577.
- [33] S. Rossi, A. Puglisi, L. M. Raimondi, M. Benaglia, *Catalysts* **2020**, *10*, 109.
- [34] S. Rossi, A. Puglisi, M. Benaglia, *ChemCatChem* **2018**, *10*, 1512–1525.
- [35] J. Li, C. Boyer, X. Zhang, *Macro. Materials & Eng.* **2022**, *307*, 2200010.
- [36] A. O. Yusuf, S. A. Jitan, R. Al Sakka, H. S. Jarusheh, C. Garlisi, L. F. Dumée, G. Palmisano, *Applied Materials Today* **2023**, *35*, 101940.
- [37] A. Hansen, M. Renner, A. G. Griesbeck, T. Büsgen, *Chem. Commun.* **2020**, *56*, 15161–15164.
- [38] D. P. Hari, B. König, *Chem. Commun.* **2014**, *50*, 6688–6699.
- [39] F. Herbrink, P. Camarero González, M. Krstic, A. Puglisi, M. Benaglia, M. A. Sanz, S. Rossi, *Applied Sciences* **2020**, *10*, 5596.
- [40] X. Li, Y. Li, Y. Huang, T. Zhang, Y. Liu, B. Yang, C. He, X. Zhou, J. Zhang, *Green Chem.* **2017**, *19*, 2925–2930.
- [41] C.-A. Wang, Y.-W. Li, X.-L. Cheng, J.-P. Zhang, Y.-F. Han, *RSC Adv.* **2017**, *7*, 408–414.
- [42] A. Sridhar, R. Rangasamy, M. Selvaraj, *New J. Chem.* **2019**, *43*, 17974–17979.
- [43] J. J. Lessard, G. M. Scheutz, A. B. Korpusik, R. A. Olson, C. A. Figg, B. S. Sumerlin, *Polym. Chem.* **2021**, *12*, 2205–2209.
- [44] F. Herbrink, S. Rossi, M. Sanz, A. Puglisi, M. Benaglia, *ChemCatChem* **2022**, *14*, e202200461.
- [45] P. F. Jacobs, *Rapid Prototyping and Manufacturing: Fundamentals of Stereolithography*, Society Of Manufacturing Engineers, Dearborn (Minn.), **1992**.
- [46] Y. Li, Q. Mao, J. Yin, Y. Wang, J. Fu, Y. Huang, *Additive Manufacturing* **2021**, *37*, 101716.
- [47] R. Chaudhary, R. Akbari, C. Antonini, *Polymers* **2023**, *15*, 287.
- [48] S. Peng, Y. Li, L. Wu, J. Zhong, Z. Weng, L. Zheng, Z. Yang, J.-T. Miao, *ACS Appl. Mater. Interfaces* **2020**, *12*, 6479–6488.
- [49] C. Kolb, N. Lindemann, H. Wolter, G. Sextl, *J. of Applied Polymer Sci* **2021**, *138*, 49691.
- [50] F. Wang, Y. Chong, F. Wang, C. He, *J. of Applied Polymer Sci* **2017**, *134*, 44988.
- [51] Y. Zhang, C. J. Ng, Z. Chen, W. Zhang, S. Panjwani, K. Kowsari, H. Y. Yang, Q. Ge, *Adv. Materials Technologies* **2019**, *4*, 1900427.
- [52] A. Alvarez-Martin, S. Trashin, M. Cuykx, A. Covaci, K. De Wael, K. Janssens, *Dyes and Pigments* **2017**, *145*, 376–384.
- [53] A. A. Ghogare, A. Greer, *Chem. Rev.* **2016**, *116*, 9994–10034.
- [54] I. Pibiri, S. Buscemi, A. Palumbo Piccionello, A. Pace, *ChemPhotoChem* **2018**, *2*, 535–547.

## COMMUNICATION

## Entry for the Table of Contents



3D-printed Eosin Y was prepared by radical photopolymerization to obtain new heterogeneous photocatalyst with a well-defined morphology. Taking advantage of the 3D-printing technology, the heterogeneous EY was designed to fit around the magnetic stirring bar to facilitate both implementation of various organic transformations and catalyst recovery. This very robust photocatalyst is easily recycled and the efficiency was still very high even after 8 reactions.